ISSN: 3064-6758 www.aristonpubs.com/scientgg-advances https://doi.org/10.69626/sea.2025.0035

RESEARCH ARTICLE

Synthesis of Zinc–Doped Iron Oxide Nanomaterials Using *Cissus Quadrangularis* : Characterizations and Photocatalytic Applications

T. Pavithra, A. Muhamed Althaf, L. Ganesh, M. Beaula Ruby Kamalam, D. Rani Roshlin, S. S. R. Inbanathan*

ABSTRACT: The growing demand for eco-friendly nanomaterials has led to an increasing focus on green synthesis approaches for metal oxide nanoparticles. In this study, iron oxide nanoparticles (IONPs) and zinc-doped iron oxide ($Zn@Fe_2O_3$) nanocomposites were synthesized using *Cissus quadrangularis* stem extract. This environmentally benign method utilizes plant-derived biomolecules as reducing, stabilizing, and capping agents. The precursor solutions of ferric nitrate and zinc nitrate were mixed with the plant extract, subjected to continuous stirring, and calcined at 500°C in a muffle furnace to obtain the final nanopowders. Structural, morphological, and optical properties of the synthesized nanomaterials were analyzed using X-ray diffraction (XRD), Fourier-transform infrared spectroscopy (FTIR), UV-Vis spectroscopy, scanning electron microscopy (SEM), and energy-dispersive X-ray spectroscopy (EDX). XRD analysis confirmed the crystalline phase of Fe_2O_3 and $Zn@Fe_2O_3$, while FTIR identified functional groups involved in nanoparticle stabilization. UV-Vis spectroscopy revealed a bandgap narrowing upon Zn doping, indicating enhanced photocatalytic potential. The photocatalytic performance was evaluated by methylene blue dye degradation under visible light irradiation, demonstrating superior efficiency for $Zn@Fe_2O_3$ compared to pure Fe_2O_3. This study highlights the potential of plant-mediated synthesis in fabricating nanomaterials with promising applications in environmental remediation. The proposed green synthesis approach offers a sustainable, cost-effective, and scalable alternative for producing metal oxide nanocomposites, reinforcing their suitability for industrial and biomedical applications.

Keywords: Green synthesis, Zinc-doped Iron oxide, *Cissus quadrangularis* stem extract, Photocatalysis.

Received: 30 July 2024; Revised: 27 September 2024; Accepted: 24 November 2024; Available Online: 15 December 2024

1. INTRODUCTION

Nanotechnology is a rapidly advancing field that has achieved significant success in modern science and technology. Among its key components, nanoparticles (NPs) exhibit unique properties due to their ultra-small size (typically 1–100 nm), high surface area, and distinct physicochemical, electrical, magnetic, thermal, mechanical, catalytic, and optical properties [1]. Unlike bulk materials with constant physical and chemical properties, nanoparticles display remarkable behavior due to their transition between atomic or molecular structures and bulk matter [2].

Nanoparticles possess a complex structure comprising three layers: the surface layer, the shell, and the core, each differing in functional groups such as metal ions, surfactants, small molecules, and polymers [3]. The unique size, shape, composition, and structural framework of nanoparticles

Department of Physics, The American College, Madurai-625002, India.

*Author to whom correspondence should be addressed: stepheninbanathan@gmail.com (S. S. R. Inbanathan)

© Ariston Publications 2025. All rights reserved.

necessitate precise optimization during synthesis to achieve desired functionalities [4]. Based on their composition and properties, nanoparticles are categorized into various types, including carbon-based, lipid-based, metallic, ceramic, semiconductor, and polymeric nanoparticles [5].

Metal oxide nanoparticles, particularly iron oxide nanoparticles (IONPs), are among the most widely studied due to their biocompatibility and superior physicochemical properties such as superparamagnetism, colloidal stability, oxidation resistance, and flexible surface chemistry [6]. These properties make IONPs highly suitable for applications in environmental remediation (e.g., pollutant detection and water treatment), catalysis, textile and electronics industries (e.g., batteries, optical devices, and gas sensors), pharmaceutical and biomedical fields (e.g., cancer therapy, drug delivery, and tissue repair), and energy storage [7].

IONPs possess a core-shell structure that contributes to their exceptional functionality, resembling both hydrous iron oxides and metallic iron [8]. They have been recognized as "nanozymes" due to their enzyme-mimicking catalytic properties, exhibiting peroxidase, catalase, sulfite oxidase, and superoxide dismutase-like activities [9]. Furthermore, these nanoparticles have a unique capability to interact with biological molecules such as peptides, enzymes, nucleic acids, lipids, and metabolites, enhancing their bioactivity and reusability [10].

Various methods have been employed for the synthesis of IONPs, including chemical, physical, and biological approaches. Chemical methods such as co-precipitation, sol-gel synthesis, hydrothermal reactions, and micro-emulsion techniques provide controlled synthesis but often involve hazardous chemicals like sodium borohydride, hydrazine, and sodium dodecyl sulfate, leading to environmental concerns [11]. Physical methods like milling, grinding, and thermal ablation demand high energy input and yield lower outputs, making them less favorable [12]. Given these limitations, the focus has shifted toward green synthesis approaches that are safer, cost-effective, and environmentally sustainable.

Green synthesis of IONPs utilizes biological entities such as plants, bacteria, fungi, algae, actinomycetes, and viruses as reducing and stabilizing agents. This approach eliminates the need for toxic chemicals, making it highly desirable for biomedical applications [13]. The biosynthesis process involves bioreduction, where metal ions are reduced to stable forms, and biosorption, where metal ions bind to biological surfaces to form stable complexes [14]. Unlike physicochemical methods, biological synthesis is time-efficient and does not require additional capping agents, as biomolecules inherently stabilize the nanoparticles [15].

This article focuses on the synthesis of IONPs using plants, discussing their advantages and limitations [16-18]. The green synthesis approach has garnered significant attention due to its eco-friendly nature, making it a promising alternative to conventional synthesis methods. In particular, IONPs have attracted considerable interest for their magnetic properties, allowing easy recovery via external magnetic fields [19, 20]. The structural diversity of biosynthesized IONPs, including cubic, spherical, elliptical, octahedral, orthorhombic, and quasi-spherical morphologies, further broadens their potential applications [16].

In this study, iron oxide nanoparticles and zinc-doped iron oxide nanocomposites were synthesized using *Cissus quadrangularis* stem extract via a green synthesis approach. Ferric nitrate and zinc nitrate were used as precursor solutions, mixed with plant extract, and stirred before drying on a hot plate. The resulting salt was ground using an agate mortar and subjected to calcination at 500°C in a muffle furnace. The synthesized samples were characterized using X-ray diffraction (XRD), Fourier-transform infrared spectroscopy (FTIR), UV-Vis spectroscopy, scanning electron microscopy (SEM), and energy-dispersive X-ray spectroscopy (EDX). The crystalline size of Fe_2O_3 nanoparticles and $Zn@Fe_2O_3$ nanocomposites was determined using XRD data, while the bandgap energy was estimated via Tauc plots. The photocatalytic efficiency was evaluated by analyzing the degradation of methylene blue dye, demonstrating the potential of these nanomaterials in environmental applications.

2. EXPERIMENTAL DETAILS

2.1. Preparation of Leaf Extract

Cissus quadrangularis plants were collected from a rural area in Madurai, India. Fresh plant stems were washed thoroughly with tap water, followed by distilled water, to remove surface contaminants and dust particles. The outer thick layer of the stems was peeled off, and the inner portion was cut into small pieces. The samples were then shade-dried at room temperature for 15 days and subsequently ground into a fine powder using an agate mortar.

For extract preparation, 15 g of plant powder was mixed with 200 mL of distilled water and heated at 80°C for 20 minutes on a hot plate. The solution was allowed to cool to room temperature and then filtered using Whatman No. 1 filter paper. The obtained extract was stored in an airtight container at room temperature for further use.

2.2. Preparation of Ferric Nitrate Precursor Solution for Iron oxide synthesis

A ferric nitrate precursor solution was prepared by dissolving 12.12 g (0.3 mol) of ferric nitrate in 100 mL of distilled water. The solution was stirred continuously on a magnetic stirrer for 30 minutes to ensure complete dissolution.

2.3. Preparation of Zinc Nitrate and Ferric Nitrate Precursor Solution

For the preparation of zinc nitrate precursor solution, 2.23 g

 © Ariston Publications 2025. All rights reserved.

of zinc nitrate was dissolved in 50 mL of distilled water and stirred for 30 minutes using a magnetic stirrer. Similarly, 9.09 g of ferric nitrate was dissolved in 50 mL of distilled water and stirred under the same conditions. The two precursor solutions were then mixed and stirred for an additional 15 minutes to obtain a homogeneous precursor solution.

2.4. Synthesis of Iron Oxide and Zinc-Doped Iron Oxide Nanoparticles

The precursor solutions were subjected to drying on a hot plate to obtain solid residues. The dried residues were ground into a fine powder using an agate mortar and pestle. The powder samples were then calcined at 500°C in a muffle furnace to complete the synthesis process. The obtained nanoparticles were characterized using various analytical techniques to assess their structural, morphological, and optical properties.

2.5. Characterization of Nanoparticles

The synthesized nanoparticles were characterized using various techniques. X-ray Diffraction (XRD) was employed to determine the crystalline structure and average crystallite size. Fourier-Transform Infrared Spectroscopy (FTIR) was used to identify functional groups and confirm biomolecule interactions. UV-Visible Spectroscopy (UV-Vis) was utilized to analyze optical properties and estimate bandgap energy using Tauc plots. Scanning Electron Microscopy (SEM) was performed to study surface morphology and particle size distribution, while Energy-Dispersive X-ray Spectroscopy (EDX) was used to determine elemental composition and confirm successful doping of zinc in iron oxide. Additionally, the photocatalytic activity of the synthesized nanoparticles was evaluated by assessing the degradation efficiency of methylene blue dye under light irradiation, highlighting their potential environmental applications.

3. RESULTS AND DISCUSSION

3.1. Characterization and properties of the nanoparticles

The structural properties of the synthesized Fe_2O_3 and $Zn@Fe_2O_3$ nanoparticles were analyzed using X-ray diffraction (XRD), as shown in Figure 1. The diffraction patterns confirmed the formation of Fe_2O_3 (Figure 1(a)) and $Zn@Fe_2O_3$ nanoparticles (Figure 1(b)) by comparing them with standard reference diffraction patterns. The XRD spectra exhibited distinct characteristic peaks corresponding to well-defined lattice planes, confirming the crystalline nature of the synthesized nanoparticles.

The diffraction peaks of the Fe_2O_3 nanoparticles were indexed to the hexagonal α-Fe_2O_3 phase, with unit cell parameters a = b = 5.0356 Å and c = 13.7489 Å, as per the standard JCPDS card No. 33-0664. The absence of peaks corresponding to Zn in the XRD patterns suggests that zinc doping did not lead to the formation of a separate zinc oxide phase. Instead, Zn^{2+} ions were likely incorporated into the Fe_2O_3 crystal lattice, as evidenced by the slight peak shifts observed in the Zn-doped samples. The XRD patterns of $Zn@Fe_2O_3$ displayed a subtle shift in diffraction peaks toward lower angles compared to pure Fe_2O_3, which suggests lattice expansion due to the incorporation of Zn^{2+} ions. Since Zn^{2+} (ionic radius ~0.74 Å) is slightly larger than Fe^{3+} (ionic radius ~0.645 Å), its substitution into the Fe_2O_3 lattice may have induced minor lattice distortions, leading to the observed peak shifts.

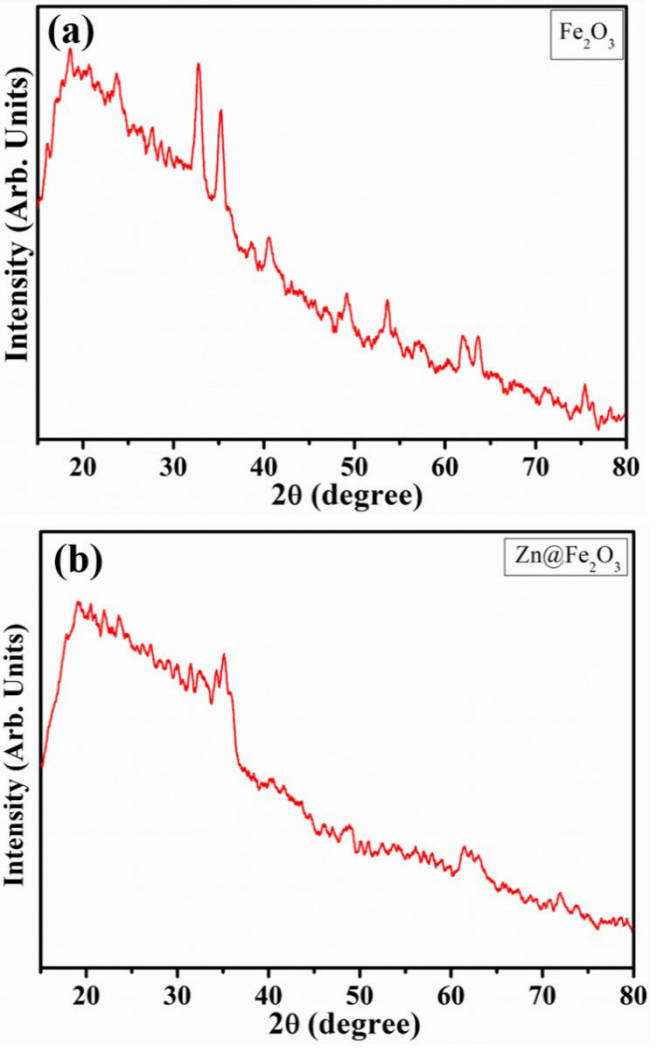


Fig. 1. XRD patterns of (a) Fe_2O_3 and (b) $Zn@Fe_2O_3$ materials.

The average crystallite size of the synthesized Fe_2O_3 and $Zn@Fe_2O_3$ nanoparticles was estimated using Scherrer's equation:

$$D = \frac{k\lambda}{\beta cos\theta} \quad (1)$$

© Ariston Publications 2025. All rights reserved.

Where D is the crystallite size, k is the shape factor (typically 0.9), λ is the X-ray wavelength, β is the full width at half maximum (FWHM) of the diffraction peak, and θ is the Bragg angle. The calculated crystallite sizes were found to be 16.14 nm for Fe_2O_3 and 5.42 nm for $Zn@Fe_2O_3$ nanoparticles, indicating that Zn doping resulted in a significant reduction in crystallite size. This reduction can be attributed to lattice strain induced by Zn incorporation, which hinders crystal growth and limits particle coarsening.

Additionally, the reduction in crystallite size with Zn doping suggests an increase in lattice defects and strain within the Fe_2O_3 structure. The presence of lattice strain can enhance surface energy and promote higher reactivity, making $Zn@Fe_2O_3$ nanoparticles more suitable for applications requiring high surface area, such as catalysis, adsorption, and environmental remediation. The absence of any additional impurity peaks further confirms the high phase purity of the synthesized samples, reinforcing the successful incorporation of Zn into the Fe_2O_3 lattice without altering its primary crystal structure.

The SEM (Scanning Electron Microscopy) and EDX (Energy Dispersive X-ray Spectroscopy) studies provide crucial insights into the morphology and elemental composition of the synthesized nanoparticles. The SEM analysis of the $Zn@Fe_2O_3$ reveals the surface structure and size distribution of the nanoparticles, highlighting their spherical or irregular shapes (Figure 2 (a)). The images from SEM confirm the presence of uniformly dispersed nanoparticles, with a consistent size range, which is an indication of successful synthesis. These images also display the surface roughness and texture of the nanoparticles, which plays a significant role in determining their reactivity and performance in various applications.

The EDX spectrum complements the SEM images by providing elemental analysis, confirming the presence of key elements, including iron (Fe), zinc (Zn), and oxygen (O), which are integral to the composition of the iron oxide and zinc-doped iron oxide nanocomposites (Figure 2 (b)). The peaks in the EDX spectrum correspond to these elements, confirming their successful incorporation into the nanoparticles. The intensity of these peaks suggests the relative concentration of each element, and the absence of unwanted impurities further validates the purity and successful doping of zinc into the iron oxide structure.

Together, the SEM and EDX results demonstrate the successful synthesis of high-quality Fe_2O_3 and $Zn@Fe_2O_3$ nanoparticles, with the desired morphology and composition. These findings are essential for understanding the relationship between the structure and the photocatalytic properties of the nanoparticles, which can be used in various applications such as pollutant degradation, water treatment, and environmental monitoring. The SEM and EDX images, therefore, not only confirm the physical attributes of the nanoparticles but also provide a detailed analysis of their elemental composition, reinforcing the effectiveness of the green synthesis method employed in this study.

Fourier transform infrared (FTIR) analysis was conducted to determine the functional groups and chemical bonding in the synthesized Fe_2O_3 and $Zn@Fe_2O_3$ nanoparticles. The FTIR spectra were recorded in the range of 400–4000 cm^{-1}, revealing distinct vibrational bands corresponding to molecular interactions and structural characteristics of the nanoparticles [21]. The FTIR spectrum of Fe_2O_3 nanoparticles, as shown in Figure 3 (a), confirmed the formation of iron oxide through characteristic absorption peaks. The spectrum displayed an absorption band at 1632 cm^{-1} and another at 1383 cm^{-1}, which correspond to the symmetric and asymmetric bending vibrations of C=O bonds. The presence of these peaks indicates the existence of carboxylate groups, likely originating from residual plant metabolites used during the green synthesis process [22].

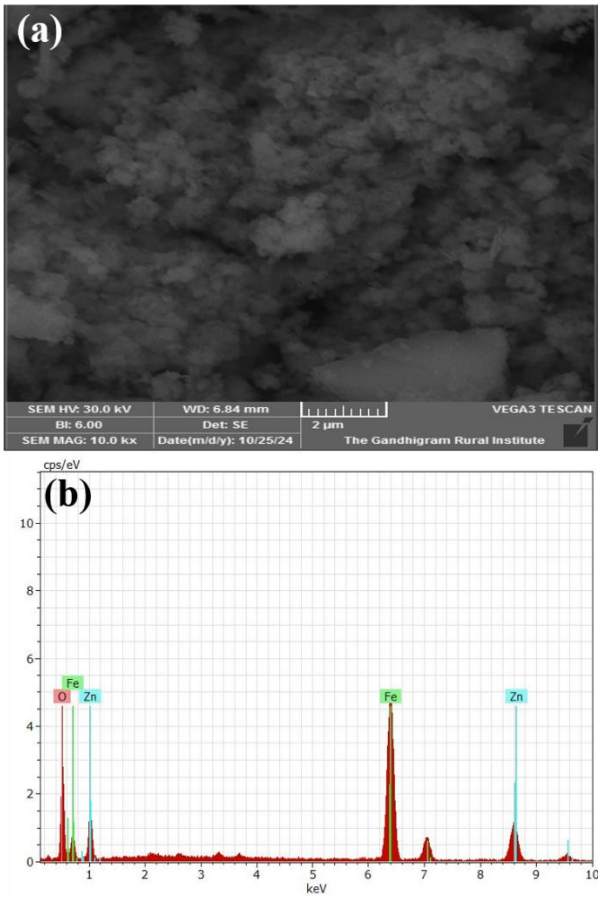


Fig. 2. (a) SEM image, and (b) EDX spectrum of $Zn@Fe_2O_3$ nanoparticles.

Additionally, a distinct peak at 1020 cm^{-1} was observed, which is attributed to C-H stretching vibrations. This suggests that organic functional groups derived from the plant extract played a role in stabilizing the nanoparticles [23]. A strong absorption band below 700 cm^{-1} was also evident, which is characteristic of the Fe-O stretching mode, confirming the successful formation of iron oxide nanoparticles [24]. The presence of organic residues in the Fe_2O_3 nanoparticles suggests that phytochemicals from *Cissus quadrangularis* extract functioned as both reducing and stabilizing agents. These phytochemicals likely

 © Ariston Publications 2025. All rights reserved.

contributed to biocompatibility while preventing nanoparticle aggregation, which is essential for maintaining stability and uniform dispersion in applications requiring controlled particle behavior [25]. The FTIR spectrum of $Zn@Fe_2O_3$ nanocomposites, presented in Fig. 4.4, revealed additional vibrational modes associated with the incorporation of zinc, which indicates structural and chemical modifications within the Fe_2O_3 lattice. The absorption band at 558 cm^{-1} corresponds to Fe-O stretching vibrations, further confirming the presence of iron oxide in the composite material [26]. Another peak, appearing at 463 cm^{-1}, is attributed to the bending vibration mode of Fe_2O_3, which verifies the structural integrity of the iron oxide framework even after zinc incorporation [27].

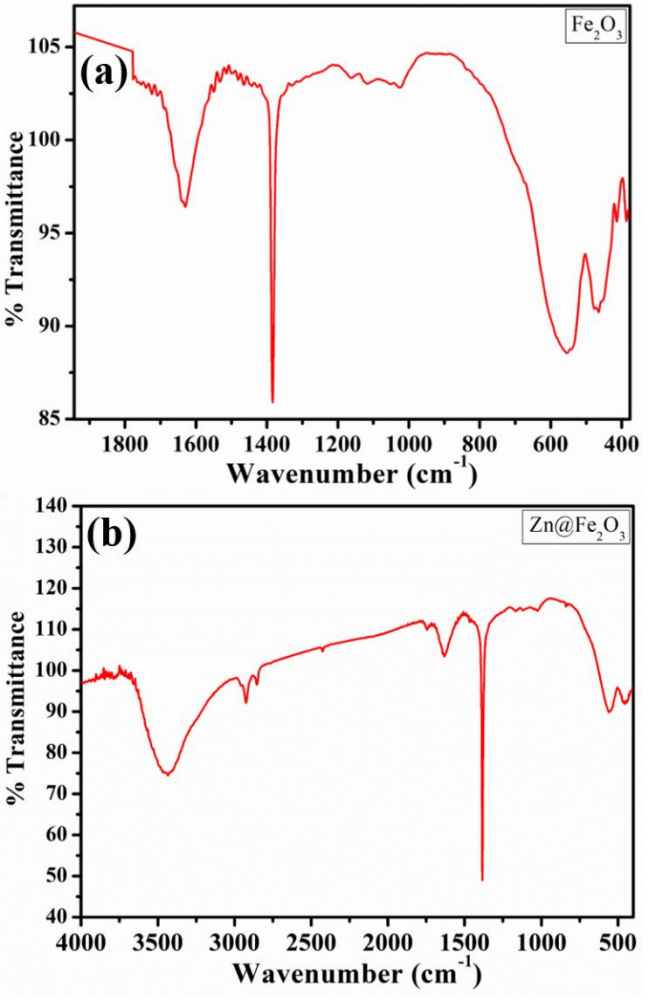


Fig. 3. FTIR spectra of (a) Fe_2O_3 and (b) $Zn@Fe_2O_3$ nanomaterials.

A broad absorption band around 3430 cm^{-1} was observed, which is assigned to O – H stretching vibrations. This suggests the presence of hydroxyl groups, potentially resulting from moisture adsorption or residual hydroxyl groups from the precursor solution [24, 25]. Additionally, peaks at 2920 cm^{-1} and 2852 cm^{-1} were identified, corresponding to asymmetric CH_2 and symmetric CH_3 stretching vibrations. These peaks suggest the presence of organic capping agents derived from the plant extract, which enhance the stability of the nanocomposites by preventing unwanted aggregation and improving dispersibility [26]. The differences in vibrational modes between Fe_2O_3 and $Zn@Fe_2O_3$ nanoparticles indicate that zinc doping influenced the local chemical environment, potentially altering bond strength and causing lattice distortions. The presence of hydroxyl and organic functional groups in the $Zn@Fe_2O_3$ nanocomposites suggests that surface modifications may have occurred, enhancing the dispersibility and reactivity of the material for various applications. Such modifications could improve the nanocomposites' efficiency in adsorption, catalysis, and biomedical applications where surface interactions play a crucial role [27].

The optical properties of the synthesized Fe_2O_3 nanoparticles were analyzed using UV-Visible absorption spectroscopy (Figure 4 (a)). A peak was observed at 252 nm for the Fe_2O_3 nanoparticles, which is consistent with the expected peak range of 240-300 nm for Fe_2O_3 [28]. Similarly, the optical properties of the $Zn@Fe_2O_3$nanoparticles were analyzed using UV-Visible absorption spectroscopy (Figure 4 (b)). The peak was obtained at 219 nm for the zinc-doped iron oxide nanoparticles, falling within the expected range of 200-290 nm for Zn-Fe_2O_3 [29]. To determine the bandgap of the synthesized nanoparticles, the Tauc plot method was employed. From the Tauc plot for Fe_2O_3, the calculated bandgap was 3.19 eV, and for $Zn@Fe_2O_3$, the bandgap was found to be 3.61 eV [30]. These values suggest an enhancement in the bandgap due to zinc doping, which is in line with previous studies [31].

3.2. Photocatalytic properties

In this study, the photocatalytic degradation of methylene blue (MB) dye was investigated using two different catalysts, Fe_2O_3 and $Zn@Fe_2O_3$, under visible light exposure (Figure 5). The experimental procedure involved preparing a 3 ppm solution of MB dye in 100 mL of distilled water, which was stirred for 30 minutes to ensure uniform dispersion. Following this, 0.01 g of Fe_2O_3 was added to the dye solution and stirred for an hour in the dark to allow the catalyst to adsorb the dye. After this adsorption period, the solution was exposed to sunlight, and the photocatalytic degradation of the dye was initiated. Samples were collected at regular intervals of 30 minutes and analyzed using UV-Visible Spectroscopy to monitor the degradation process. The same procedure was repeated using $Zn@Fe_2O_3$ nanoparticles as the catalyst [31].

The results of the photocatalytic degradation for both Fe_2O_3 (Figure 5 (a)) and $Zn@Fe_2O_3$ (Figure 5 (b)) nanoparticles are shown graphically, depicting the dye degradation as a function of time. As the reaction progressed, the intensity of the characteristic absorption peaks of methylene blue decreased, which correlates with the degradation of the dye. The spectral analysis revealed that $Zn@Fe_2O_3$ nanoparticles exhibited superior photocatalytic performance compared to Fe_2O_3 nanoparticles [30-31].

© Ariston Publications 2025. All rights reserved.

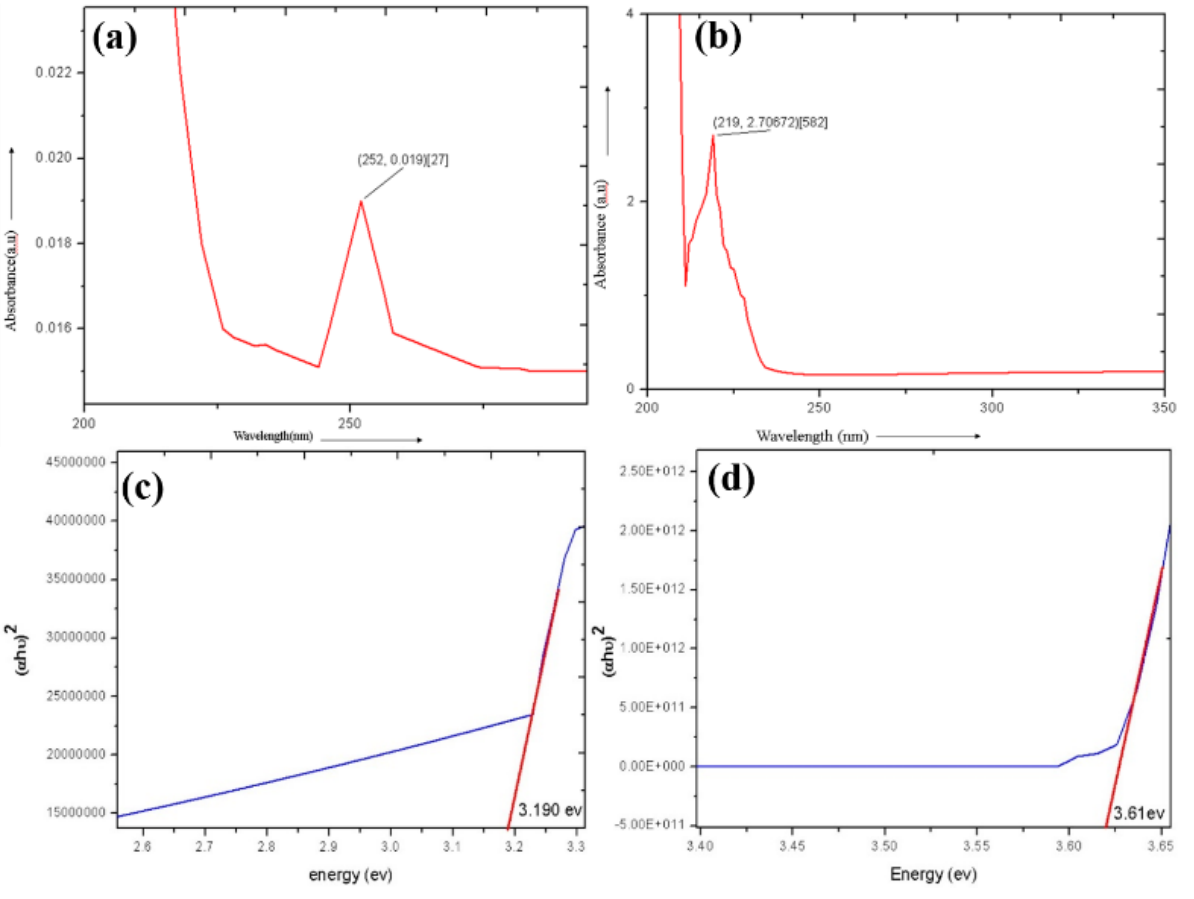


Fig. 4. UV-Visible spectra for (a) Fe_2O_3, (b) $Zn@Fe_2O_3$, and Tauc plots for (c) Fe_2O_3, (d) $Zn@Fe_2O_3$.

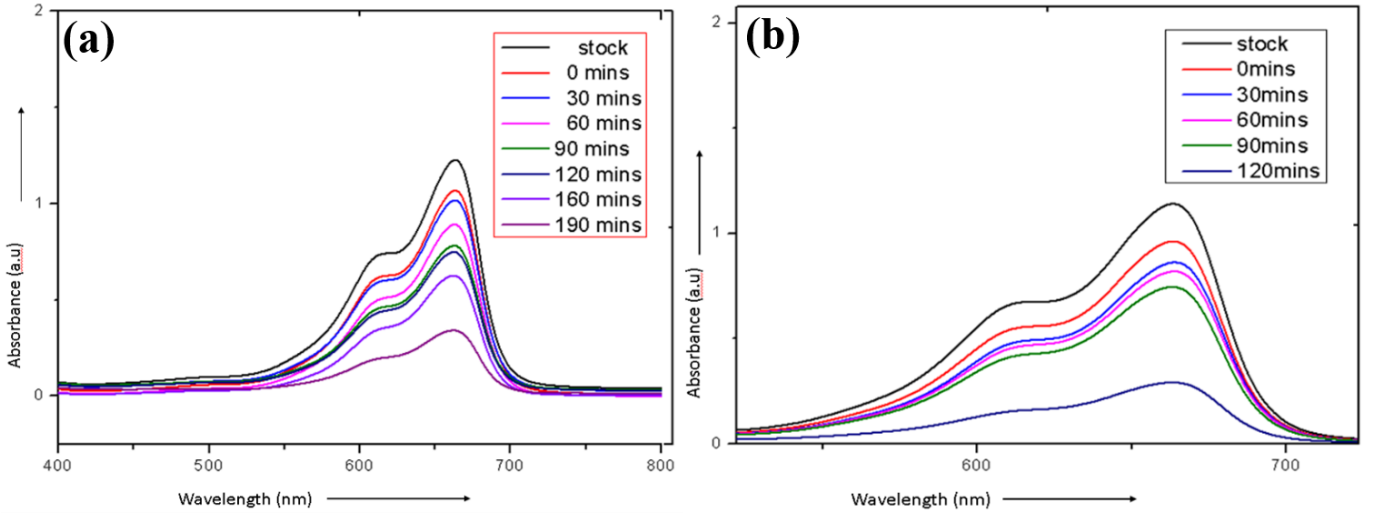


Fig. 5. Visible-light driven photocatalytic degradation of MB dye based on (a) Fe_2O_3, and (b) $Zn@Fe_2O_3$ nanoparticles.

This is evident from the faster and more extensive degradation observed in the presence of $Zn@Fe_2O_3$.

The efficiency of dye degradation was calculated based on the reduction in the absorption intensity of the MB dye over time. For the Fe_2O_3 catalyst, the dye degradation efficiency was found to be 29%, whereas the $Zn@Fe_2O_3$ catalyst achieved a significantly higher degradation efficiency of 69%. This indicates that the Zn-doped Fe_2O_3 nanoparticles are more effective in promoting the photocatalytic degradation of methylene blue dye under visible light conditions.

Several factors could explain the enhanced

 © Ariston Publications 2025. All rights reserved.

photocatalytic performance of Zn@Fe_2O_3 nanoparticles. The doping of zinc into the Fe_2O_3 structure likely improves the electronic properties of the catalyst, such as its bandgap and charge separation efficiency. Zinc doping can increase the generation of reactive oxygen species (ROS), such as hydroxyl radicals (•OH) and superoxide anions (O^{2}•−), which are responsible for the degradation of organic pollutants like methylene blue. Furthermore, the Zn@Fe_2O_3nanoparticles may exhibit better light absorption properties due to the narrowing of the bandgap, which enhances their photocatalytic activity under visible light exposure.

The comparison between Fe_2O_3 and Zn@Fe_2O_3 highlights the potential of doping strategies to enhance the photocatalytic performance of metal oxide nanoparticles. The higher degradation efficiency of Zn@Fe_2O_3suggests its promising application in environmental remediation, particularly for the degradation of organic pollutants in water. These results also indicate the importance of optimizing the synthesis and doping processes to achieve the best photocatalytic performance for real-world applications.

4. CONCLUSION

The present study successfully demonstrates the green synthesis of iron oxide nanoparticles (Fe_2O_3) and zinc-doped iron oxide (Zn@Fe_2O_3) nanocomposites using *Cissus quadrangularis* stem extract. This eco-friendly synthesis method eliminates the need for toxic chemicals and energy-intensive procedures, making it an attractive alternative for nanomaterial production. Structural characterization using XRD confirmed the crystalline nature of the nanoparticles, while FTIR analysis validated the presence of plant-derived functional groups that played a crucial role in nanoparticle stabilization. SEM and EDX analyses further affirmed the morphological integrity and elemental composition of the synthesized nanomaterials. The optical properties of Fe_2O_3 and Zn@Fe_2O_3, as revealed by UV-Vis spectroscopy, indicated a bandgap reduction upon Zn doping, enhancing their potential for photocatalytic applications. The photocatalytic degradation of methylene blue under visible light irradiation showcased remarkable efficiency for Zn@Fe_2O_3, demonstrating its superior ability to break down organic pollutants compared to undoped Fe_2O_3. This suggests that Zn doping significantly enhances the catalytic performance of iron oxide nanoparticles, making them promising candidates for environmental remediation. This study underscores the significance of biological routes for nanoparticle synthesis, providing a sustainable and cost-effective alternative to conventional chemical and physical methods. The use of plant-based synthesis not only ensures biocompatibility but also enhances the structural and functional properties of nanomaterials. Future research should explore the scalability of this synthesis approach, its applicability to other metal oxide systems, and its potential in biomedical and industrial applications. The findings presented here pave the way for the development of next-generation eco-friendly nanomaterials with enhanced photocatalytic and environmental remediation capabilities.

DECLARATIONS

Ethical Approval

We affirm that this manuscript is an original work, has not been previously published, and is not currently under consideration for publication in any other journal or conference proceedings. All authors have reviewed and approved the manuscript, and the order of authorship has been mutually agreed upon.

Funding

Not applicable

Availability of data and material

All of the data obtained or analyzed during this study is included in the report that was submitted.

Conflicts of Interest

The authors declare that they have no financial or personal interests that could have influenced the research and findings presented in this paper. The authors alone are responsible for the content and writing of this article.

Authors' contributions

All authors contributed equally in the preparation of this manuscript.

ACKNOWLEDGEMENTS

Authors acknowledge the research facilities of The American College, Madurai, India. One of the authors S.S.R Inbanathan acknowledges the grant (TNSCST/STP/2021-22/ES-02/VR/2023) received from Tamilnadu State Council for Science and Technology,India for carrying out this research.

REFERENCES

[1] Kiwumulo, H.F., Muwonge, H., Ibingira, C., Lubwama, M., Kirabira, J.B. and Ssekitoleko, R.T., **2022.** Green synthesis and characterization of iron-oxide nanoparticles using Moringa oleifera: a potential protocol for use in low and middle income countries. *BMC Research Notes*, *15*(1), p.149.

[2] Kasparis, G., Sangnier, A.P., Wang, L., Efstathiou, C.,

© Ariston Publications 2025. All rights reserved.

LaGrow, A.P., Sergides, A., Wilhelm, C. and Thanh, N.T.K., **2023**. Zn doped iron oxide nanoparticles with high magnetization and photothermal efficiency for cancer treatment. *Journal of Materials Chemistry B*, *11*(4), pp.787-801.

[3] Abdulrahaman, M.D., Faruk, N., Oloyede, A.A., Surajudeen-Bakinde, N.T., Olawoyin, L.A., Mejabi, O.V., Imam-Fulani, Y.O., Fahm, A.O. and Azeez, A.L., **2020**. Multimedia tools in the teaching and learning processes: A systematic review. *Heliyon*, *6*(11), p. e05312.

[4] Kasparis, G., Sangnier, A.P., Wang, L., Efstathiou, C., LaGrow, A.P., Sergides, A., Wilhelm, C. and Thanh, N.T.K., **2023**. Zn doped iron oxide nanoparticles with high magnetization and photothermal efficiency for cancer treatment. *Journal of Materials Chemistry B*, *11*(4), pp.787-801.

[5] Sathappan, S., Kirubakaran, N., Gunasekaran, D., Gupta, P.K., Verma, R.S. and Sundaram, J., **2021**. Green synthesis of zinc oxide nanoparticles (ZnO NPs) using cissus quadrangularis: Characterization, antimicrobial and anticancer studies. *Proceedings of the National Academy of Sciences, India Section B: Biological Sciences*, *91*, pp.289-296.

[6] Naiel, B., Fawzy, M., Halmy, M.W.A. and Mahmoud, A.E.D., **2022**. Green synthesis of zinc oxide nanoparticles using Sea Lavender (Limonium pruinosum L. Chaz.) extract: characterization, evaluation of anti-skin cancer, antimicrobial and antioxidant potentials. *Scientific Reports*, *12*(1), p.20370.

[7] Loganathan, S., Shivakumar, M.S., Karthi, S., Nathan, S.S. and Selvam, K., **2021**. Metal oxide nanoparticle synthesis (ZnO-NPs) of Knoxia sumatrensis (Retz.) DC. Aqueous leaf extract and It's evaluation of their antioxidant, anti-proliferative and larvicidal activities. *Toxicology Reports*, *8*, pp.64-72.

[8] Mahmoud, A.E.D., El-Maghrabi, N., Hosny, M. and Fawzy, M., **2022.** Biogenic synthesis of reduced graphene oxide from Ziziphus spina-christi (Christ's thorn jujube) extracts for catalytic, antimicrobial, and antioxidant potentialities. *Environmental Science and Pollution Research*, *29*(59), pp.89772-89787.

[9] Berehu, H.M., S, A., Khan, M.I., Chakraborty, R., Lavudi, K., Penchalaneni, J., Mohapatra, B., Mishra, A. and Patnaik, S., **2021.** Cytotoxic potential of biogenic zinc oxide nanoparticles synthesized from swertia chirayita leaf extract on colorectal cancer cells. *Frontiers in Bioengineering and Biotechnology*, *9*, p.788527.

[10] Smijs, T.G. and Pavel, S., **2011.** Titanium dioxide and zinc oxide nanoparticles in sunscreens: focus on their safety and effectiveness. *Nanotechnology, Science and Applications*, pp.95-112.

[11] Kaushik, M., Niranjan, R., Thangam, R., Madhan, B., Pandiyarasan, V., Ramachandran, C., Oh, D.H. and Venkatasubbu, G.D., **2019**. Investigations on the antimicrobial activity and wound healing potential of ZnO nanoparticles. *Applied Surface Science*, *479*, pp.1169-1177.

[12] Hosny, M., Fawzy, M., Abdelfatah, A.M., Fawzy, E.E. and Eltaweil, A.S., **2021**. Comparative study on the potentialities of two halophytic species in the green synthesis of gold nanoparticles and their anticancer, antioxidant and catalytic efficiencies. *Advanced Powder Technology*, *32*(9), pp.3220-3233.

[13] Manousaki, E. and Kalogerakis, N., **2011**. Halophytes present new opportunities in phytoremediation of heavy metals and saline soils. *Industrial & Engineering Chemistry Research*, *50*(2), pp.656-660.

[14] Zengin, G., Aumeeruddy-Elalfi, Z., Mollica, A., Yilmaz, M.A. and Mahomoodally, M.F., **2018**. In vitro and in silico perspectives on biological and phytochemical profile of three halophyte species—A source of innovative phytopharmaceuticals from nature. *Phytomedicine*, *38*, pp.35-44.

[15] Ogbole, O.O., Segun, P.A. and Adeniji, A.J., **2017.** In vitro cytotoxic activity of medicinal plants from Nigeria ethnomedicine on Rhabdomyosarcoma cancer cell line and HPLC analysis of active extracts. *BMC Complementary and Alternative Medicine*, *17*, pp.1-10.

[16] López-Cuenca, S., Pérez Carrillo, L.A., Rabelero Velasco, M., Díaz de León, R., Saade, H., López, R.G., Mendizábal, E. and Puig, J.E., **2011.** High-yield synthesis of zinc oxide nanoparticles from bicontinuous microemulsions. *Journal of Nanomaterials*, *2011*(1), p.431382.

[17] Sajadi, S.M., Kolo, K., Pirouei, M., Mahmud, S.A., Ali, J.A. and Hamad, S.M., **2018.** Natural iron ore as a novel substrate for the biosynthesis of bioactive-stable ZnO@ CuO@ iron ore NCs: a magnetically recyclable and reusable superior nanocatalyst for the degradation of organic dyes, reduction of Cr (vi) and adsorption of crude oil aromatic compounds, including PAHs. *RSC advances*, *8*(62), pp.35557-35570.

[18] Meena, P.L., Poswal, K. and Surela, A.K., **2022**. Facile synthesis of ZnO nanoparticles for the effective photodegradation of malachite green dye in aqueous solution. *Water and Environment Journal*, *36*(3), pp.513-524.

[19] Adams, R.P., **2017.** Identification of essential oil components by gas chromatography/mass spectrometry. 5 online ed. *Gruver, TX USA: Texensis Publishing*, pp.46-52.

[20] Barzinjy, A.A. and Azeez, H.H., **2020.** Green synthesis and characterization of zinc oxide nanoparticles using Eucalyptus globulus Labill. leaf extract and zinc nitrate hexahydrate salt. *SN Applied Sciences*, *2*(5), p.991.

[21] Wei, K., Zhao, S., Zhang, W., Zhong, X., Li, T., Cui, B., Gao, S., Wei, D. and Shen, Y., **2019.** Controllable synthesis of Zn-doped α-Fe_2O_3 nanowires for H_2S sensing. *Nanomaterials*, *9*(7), p.994.

[22] Zhao, H., Li, J., She, X., Chen, Y., Wang, Y., Zou, C. and Zhou, Y., **2023.** Black phosphorus nanosheets-sensitized Zn-doped α-Fe_2O_3 nanoclusters for trace acetone detection. *Sensors and Actuators B:*

 © Ariston Publications 2025. All rights reserved.

Chemical, *395*, p.134496.

[23] Hu, J.Y., Lei, H., Zhang, H.Y., Xue, X.X., Wang, X.P., Wang, C.H. and Zhang, Y., **2024.** High reliable gas sensor based on crystal-facet regulated α-Fe_2O_3 nanocrystals for rapid detection of exhaled acetone. *Rare Metals*, *43*(12), pp.6500-6515.

[24] Liu, D., Li, X., Li, Y., Yin, S., Liu, J. and Zhang, J., **2022.** Fe-functionalized α-Fe_2O_3/ZnO nanocages for ppb-level acetone gas sensing. *ACS Applied Nano Materials*, *5*(4), pp.5745-5755.

[25] Suman, Chahal, S., Kumar, A. and Kumar, P., **2020**. Zn doped α-Fe_2O_3: an efficient material for UV driven photocatalysis and electrical conductivity. *Crystals*, *10* (4), p.273.

[26] Kumar, P., Sharma, V., Singh, J.P., Kumar, A., Chahal, S., Sachdev, K., Chae, K.H., Kumar, A., Asokan, K. and Kanjilal, D., **2019**. Investigations on magnetic and electrical properties of Zn doped Fe_2O_3 nanoparticles and their correlation with local electronic structures. *Journal of Magnetism and Magnetic Materials*, *489*, p.165398.

[27] Song, H., Sun, Y. and Jia, X., **2015**. Hydrothermal synthesis, growth mechanism and gas sensing properties of Zn-doped α-Fe_2O_3 microcubes. *Ceramics International*, *41*(10), pp.13224-13231.

[28] Shi, D., Sadat, M.E., Dunn, A.W. and Mast, D.B., **2015.** Photo-fluorescent and magnetic properties of iron oxide nanoparticles for biomedical applications. *Nanoscale*, *7* (18), pp.8209-8232.

[29] Badawi, A., Althobaiti, M.G., Alharthi, S.S., Alharbi, A.N., Alkathiri, A.A. and Alomairy, S.E., **2022.** Effect of zinc doping on the structure and optical properties of iron oxide nanostructured films prepared by spray pyrolysis technique. *Applied Physics A*, *128*(2), p.123.

[30] Lassoued, A., **2021**. Synthesis and characterization of Zn-doped α-Fe_2O_3 nanoparticles with enhanced photocatalytic activities. *Journal of Molecular Structure*, *1239*, p.130489.

[31] Joseph, J.A., Nair, S.B., John, S.S., Remillard, S.K., Shaji, S. and Philip, R.R., **2021**. Zinc-doped iron oxide nanostructures for enhanced photocatalytic and antimicrobial applications. *Journal of Applied Electrochemistry*, *51*, pp.521-538.

© Ariston Publications 2025. All rights reserved.